High-Temperature Effects on Aerodynamic and Acoustics Characteristics of a Rectangular Supersonic Jet

Song Chen, Romain Gojon, Mihai Mihaescu

AIAA AVIATION Forum
June 25-29, 2018, Atlanta, Georgia
2018 AIAA/CEAS Aeroacoustics Conference

High-Temperature Effects on Aerodynamic and Acoustics Characteristics of a Rectangular Supersonic Jet

Song Chen*, Romain Gojon†, Mihai Mihaescu‡

KTH Royal Institute of Technology
Stockholm, Sweden, 10044

Implicit large-eddy simulations (LES) are performed in this work to study the flow field and acoustic characteristics of a rectangular supersonic jet. The focus is to investigate the high-temperature effects, i.e. when the jet total temperature is as high as 2100 K. Four cases with a jet temperature ratio(TR) of 1.0, 2.0, 4.0 and 7.0 are investigated. The rectangular nozzle selected for this study has an aspect ratio of 2. The jets are overexpanded, with a series of shock cells in the jet core region. An artificial dissipation mechanism is used to damp the numerical oscillation and to represent the effect of small-scale turbulence. The temperature-dependent thermal properties of air within the high-temperature regime are also considered by using the chemical equilibrium assumption. The numerical results show that the high temperature significantly increases the jet velocity and acoustic Mach number, although the jet Mach number is maintained roughly the same. Meanwhile, the length of the jet core region of the hot jet (TR = 7.0) is found to be reduced by around 30 %, compared to the cold jet. The convection velocity and acoustic convection Mach number in the shear layer are also observed to be increased when the jet temperature is high. The elevated acoustic convection Mach number directly leads to a strong Mach wave radiation, and the crackle noise component has been identified by the pressure skewness and kurtosis factors. The Strouhal number of the screech tone is found to be decreased slightly, and good agreements between the numerical results and the theoretical analysis are observed. Moreover, the sound pressure levels (SPL) associated with turbulent mixing, screech, Mach wave radiation, and Broadband shock associated noise are all found to be amplified in different levels for the hot jets. In the far field, the SPL are strongly affected and increased by the high-temperature effect. Higher levels are notably observed in the side, downstream, and especially the Mach wave radiation directions.

I. Introduction

Rectangular propulsion systems, compared with their axisymmetric opponents, have been proved to be more suitable for future high-speed aircrafts because of a number of attractive features, for example, reduction of drag due to a better integration to the airframe, ease of design and manufacture as relatively few components are needed for the thrust vector control [1, 2], and increased entrainment and mixing performance of the exhausting jet [3]. Among many research interests in this type of high-performance engine, supersonic jet noise has been a hot topic for the past several decades, mainly aiming to understand the noise generation mechanism, to develop and optimize effective noise reduction techniques, and to mitigate its adverse effects on personnel working with aircraft engines or residents in close proximity to airports.

The main components that contribute to the supersonic jet noise include the turbulent mixing noise, the Mach wave radiation, the broadband shock-associated noise, and the screech noise [4–6]. The turbulent mixing noise is generated by both the large turbulent coherent structures near the end of the jet potential core and the fine-scale turbulence in the shear layer. In a supersonic jet, the large turbulence scales dominate and they radiate the mixing noise into an angular sector of about 120 - 160 degrees measured from the jet upstream direction. The Mach wave radiation can be explained by the wavy wall analogy. In this analogy, large-scale turbulent structures of the shear layer can be treated as wavy walls. The wavy wall is convected downstream at a supersonic speed, and compression waves are generated and attached to it. The propagation direction of the Mach wave radiations can thus be estimated by using the Mach angle relation based on the convective supersonic velocity and the local speed of sound. The broadband shock-associated

*Postdoctoral Researcher, Department of Mechanics, Linné FLOW Centre; sonc@mech.kth.se
†Postdoctoral Researcher, Department of Mechanics, Linné FLOW Centre; also Research Associate at Département Aérodynamique, Energétique et Propulsion-DAEP ISAESUPAERO, Université de Toulouse, 10 Avenue Edouard Belin, 31400 Toulouse, France; romain.gojon@isae-supaero.fr
‡Associate Professor, Department of Mechanics, Linné FLOW Centre, Senior Member AIAA; mihai@mech.kth.edu

noise, first identified by Harper-Bourne and Fisher [7], is generated by the interactions between a quasi-periodic shock cell structure in the jet core and turbulent flow structures in the jet shear layer. The screech noise, first observed by Powell [8,9], is characterized by strong and discrete tones. This noise component is generated by an acoustic feedback mechanism in the mixing layer which includes downstream convected turbulent vortical structures from the lip of nozzle and upstream propagating acoustic waves generated by the interaction between perturbations and shock cells. The screech tones are primarily radiated in the upstream direction.

Understanding of the supersonic jet noise currently still strongly relies on jet experiments, such as the work from Mora et al. [10] and Wall et al. [11]. These experimental data not only provide reliable data to obtain insights of noise generation mechanism but also can act as a benchmark for further numerical simulations which may offer more detailed information. However, the present scaled laboratory experiment is facing difficulties of long-duration testing in the high-temperature regime, which can be as high as 2000 K for high-performance engines with an afterburner. Under such high temperatures, experimental rigs simply melt. This applies to certain types of data acquisition systems as well, such as the intrusive flow measurement tool Pitot tube. LES, which has the ability to resolve the turbulent structures that are important to the noise generation but is not limited by the high-temperature constraints, becomes a reliable and promising method to investigate and understand the effects of high temperatures.

Tam et al. [12,13] reported that jet noise can be affected by hot temperatures from two perspectives: a large density gradient and an increased convective Mach number. The large density gradient in a hot jet has a strong influence on both the mean flow and the turbulent mixing noise. When the jet is heated to high temperatures, the density difference between the jet and ambient cold air tend to enhance the Kelvin-Helmholtz instability [14], which promotes turbulent mixing as well as the jet spreading rate. However, the increased convective Mach number is known to stabilize turbulent mixing [15], which tends to counterbalance the density gradient effect. Compared with cold jets, it has also been found that hot jets have a shorter eddy decay time and slightly reduced eddy size which may greatly affect noise radiations [16]. Viswanathan [17] systematically studied the effect of jet temperature on the noise radiation in subsonic jets. It was found that the shift of the spectral shape observed in hot jets is due to the Reynolds number effect instead of extra dipole sources that had been mistakenly concluded previously. Moreover, when the Reynolds number exceeds 4.0×10^5, its effect on acoustic characteristics can almost be neglected [17].

Cacqueray and Bogey [18] analyzed the LES data of a supersonic jet with a total temperature of 1144 K. It was found that the strong non-linear effects resulted in a series of N-shaped waves in the pressure signals. Langenais et al. [19] numerically investigated a supersonic jet with a total temperature of 1900 K. The coupled CFD-CAA method used in this work was found to be able to significantly improve the numerical predictions compared to the use of the classical Ffowcs Williams-Hawkings (FW-H) analogy, especially when the acoustics level is high enough to trigger nonlinear effects. Gojon et al. [20] numerically investigated the temperature effect on the aerodynamic and acoustic fields of a rectangular supersonic jet through LES. In his work, different temperature ratios ($T_t/T_{ambient}$, where T_t and $T_{ambient}$ are the total temperature for the jet and ambient air respectively) ranging from 1.0 to 3.0 (from 293 K to 879 K for the total temperature) were considered for a slightly overexpanded supersonic jet. It was found that the shock structures of the jet were affected by the temperature, and the number of shock cells decreased when the jet temperature was increased. The Overall Sound Pressure Level (OASPL) revealed an intensified screech feedback mechanism when the temperature was increased and strong flapping motions of the jet along the minor axis were observed. Liu et al. [21–23] conducted a numerical campaign to study the aeroacoustic characteristics of highly heated supersonic jets using LES with a temperature ratio up to 7.0 (about 2100 K), which almost matches with the exhausting jet temperature from a high-performance engine with an afterburner. Through investigating the effects of the specific heat ratio, it was found that the assumption of a constant specific heat ratio of 1.4 in high-temperature jets would introduce a lower nozzle-exit pressure and a weaker shock-cell structure, which lead to an underestimated noise intensity (about 1~2 dB) in the upstream direction over the entire frequency range. It was also observed that the cold jet only displayed a single downstream lobe in the far-field noise distribution, whereas high-temperature jets showed a dual lobe pattern. Furthermore, the peak radiation direction of the OASPL was found to shift upstream when the jet temperature increases. The work of Neilsen et al. [24] and Tam and Parrish [25] reveal that there is a new dominant noise component for the high-performance aircraft engine at afterburner operating conditions. The new noise component is dominant in the angular directions between 110 and 130 degrees and for a frequency above 200 Hz. Tam and Parrish believed this new component was most probably indirect combustion noise generated by entropy waves [26] coming out the afterburner through the nozzle. However, the understanding of this new noise component and its generation mechanism is still limited.

To the best of the authors' knowledge, there are not many numerical studies on the flow and acoustics fields of supersonic jets with a temperature up to 2000 K. There is a crucial need to understand the non-linear propagation effects and the newly revealed noise components in high-performance engines. The present paper, as a continuation of our previous work [20], will continue to focus on the temperature effect on aerodynamic and acoustic characteristics of

a rectangular supersonic jet. But the temperature ratio of interest is extended from the previous relatively low regime of 1.0 - 3.0 to a high regime of 4.0 - 7.0, which is a more representative for the practical high-performance jet engine. This paper is organized in the following way: section II describes the nozzle geometry and operating conditions; flow solver and numerical methods are illustrated in section III; information of verification and validation is in section IV; numerical results and discussion are presented in section V and VI; conclusion is given in section VII.

II. Nozzle Geometry and Operating Conditions

A converging-diverging (C-D) bi-conic rectangular nozzle previously studied by Gojon et al. [20, 27] is selected for this work. The working fluid for the jet in this paper is air. The rectangular nozzle has an aspect ratio of 2.0 and a C-D profile on the major walls. With an area ratio (A_e/A^*) of 1.18, the nozzle has a design Mach number of 1.5 that corresponds to a nozzle pressure ratio (NPR) of 3.67. More detailed information about the nozzle geometry and operating conditions can be found in Ref. [10, 28–30].

In this study, a slightly overexpanded nozzle operating condition with an NPR of 3.0 is selected with four different temperature ratios (TR) of 1.0, 2.0, 4.0, and 7.0, where the ambient pressure and temperature are $P_{ambient}$=101325 Pa and $T_{ambient}$=293 K. These cases are referred to as JetTR1, JetTR2, JetTR4, and JetTR7 respectively. Details of the nozzle operating conditions are shown in Table 1. It can be seen that although the ideally expanded Mach number roughly keeps the same when TR increases (the small difference is due to the variance of γ), the ideally expanded jet velocity u_j and static temperature T_j increase significantly as well. On the contrary, Re decreases dramatically due to the greatly elevated viscosity at high temperatures.

Table 1. Nozzle operating conditions. NPR is nozzle pressure ratio; TR is temperature ratio; M_j, u_j, and T_j denote ideally expanded Mach number, velocity, and static temperature of the jet; Re is the Reynolds number computed with the jet equivalent diameter D_{eq}. This diameter is computed by converting the rectangular nozzle into a round nozzle with a same nozzle exit area.

Case	NPR	TR	M_j	$u_j(m \cdot s^{-1})$	$T_j(K)$	Re
JetTR1	3.0	1.0	1.36	399	214	9.61×10^5
JetTR2	3.0	2.0	1.36	564	430	3.96×10^5
JetTR4	3.0	4.0	1.37	801	885	1.67×10^5
JetTR7	3.0	7.0	1.39	1070	1592	0.85×10^5

The maximum temperature of the jet is around 2100 K, which is close to the total temperature of a real high-performance engine. For such a high temperature, air starts to disassociate and the composition of air changes. This can change the properties of gaseous mixture significantly (for example, the specific heat by constant pressure c_p, the specific heat by constant volume c_v, and the specific heat ratio γ) and thus affect the flow and acoustic fields predicted by CFD. Based on Liu et al. [23], a temperature-dependent specific heat ratio is recommended for the numerical study of a highly heated jet with a temperature around 2000 K. Therefore, a similar treatment with suitable air properties is adopted here. The working fluid, air, is treated as a single gas. The chemical reactions involved in the disassociation process within the high-temperature range are neglected during the simulations for simplicity. However, the temperature-dependent thermodynamic properties of air are considered by introducing a table precalculated by the chemical equilibrium computation [31]. The profiles of the specific heat ratio at different pressure are shown in Fig. 1. As the nozzle NPR is 3.0 in this work, the static pressure in the whole computational domain roughly ranges from 1 atm to 3 atm. It can be seen that there is only a tiny difference ($< 0.5\%$) between the different pressure in the high-temperature regime. Therefore, it is safe to assume the profile at 3 atm for the whole flow field computations. Moreover, the temperature dependence of viscosity μ is estimated by using Sutherland's law.

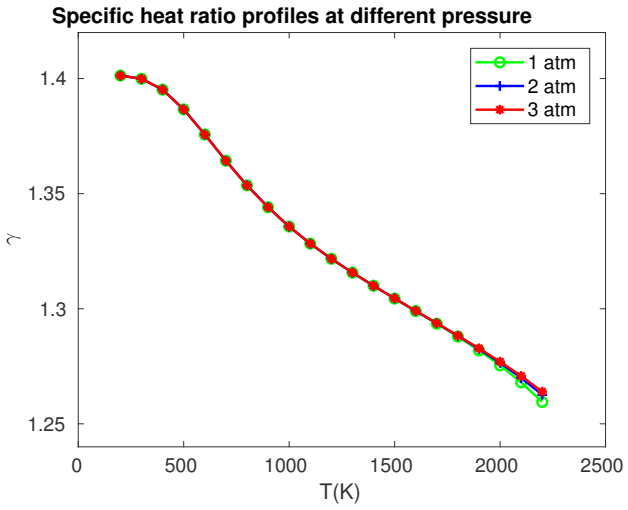

Figure 1. Temperature dependent profiles of the specific heat ratio at different pressure.

III. Computational Methodology

A. Numerical methods

Simulations in this study are performed by using a compressible flow solver [32] that has been validated and implemented in previous studies by Semlitsch et al. [33,34] and Gojon et al. [20,27]. This code uses a finite volume method to solve the three-dimensional compressible unsteady Navier-Stokes equations with the LES approach in Cartesian coordinates. In the explicit LES, large-scale eddies in the energy-containing range and a proportion of the inertial subrange filtered by the numerical mesh are resolved, while the subgrid scales (SGS) are modeled. In this paper, however, the implicit LES method [35, 36] is adopted in which no explicit filter and no explicit SGS model are applied. The small scales are assumed to be represented implicitly by the numerical dissipation, where the dissipative truncation error acts as a Smagorinsky-type SGS model. This approach is also known as monotonically integrated large eddy simulation (MILES) [37].

In the current solver, an explicit standard four-stage Runge-Kutta algorithm is used for time integration and a second-order central difference scheme is used for spatial discretization. A Jameson-type [38] artificial dissipation is added to the flow at the end of each time step. This dissipation term handles the subgrid scales as the SGS model does in the explicit LES, and it is also able to provide non-oscillatory behaviour of the second order central difference scheme near sharp gradients. Additionally, this dissipation term has been further modified based on the work of Ducros et al. [39] to better capture shocks. Details of the artificial dissipation term implemented in the study can be found in the work of Gojon et al. [20].

B. Computational domain and boundary conditions

The computational domain is shown in Fig. 2. A rectangular nozzle highlighted by the blue color is enclosed with a large cylindrical domain. The flow direction is from the left to the right, and the nozzle inlet is highlighted by the orange color. In the jet streamwise direction, the length of the enclosing domain is around $67h$, where h is the nozzle height in the minor axis plane. In the radial direction, the radius of the domain is around $21h$. Total flow conditions that specify the total pressure and total temperature are employed at the nozzle inflow boundary. The nozzle wall is assumed to be adiabatic and non-slip. The surrounding of the computational domain is set as the characteristics boundary with ambient static pressure and temperature. Together with the usage of sponge zones, those boundary conditions permit to avoid spurious reflections at the boundaries.

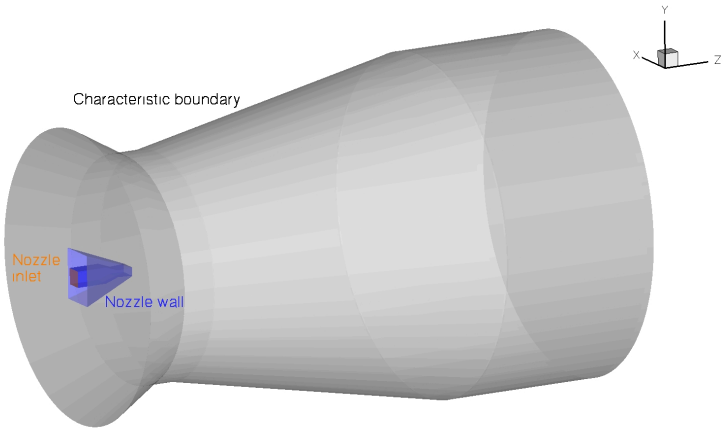

Figure 2. Schematic of the computational domain with the rectangular C-D nozzle.

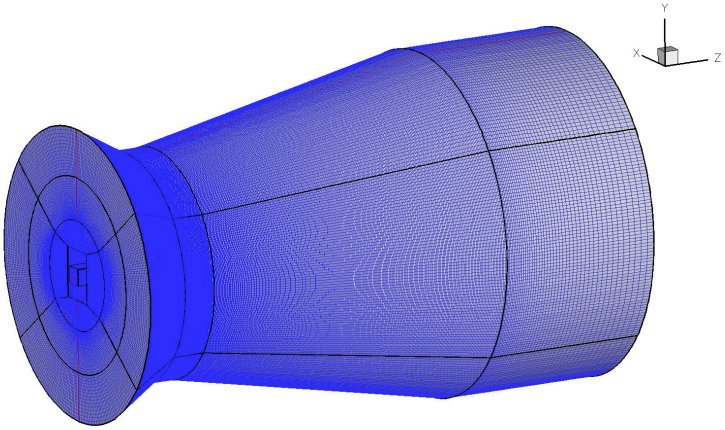

Figure 3. Schematic of the mesh (number of points have been reduced for clarity).

The schematic of the mesh used for this study is shown in Fig. 3. It is a multi-block structured mesh created by ANSYS ICEM CFD. The mesh used in this work has around 160 million cells in total and has been evaluated in our previous grid-convergence study [20]. The grid points are clustered in the jet region where large flow gradients exist, and it is stretched slowly in both the axial and radial directions. The current mesh has a small first layer thickness with a y^+ ~1 in the wall normal direction and $x^+, y^+ < 10$ in the wall parallel directions within the diverging part of the nozzle. The growth ratio of the grid is controlled below 5 % to avoid high dissipation or dispersion errors from the spatial derivation scheme.

The computations on the grid with 160 million cells are performed on 960 processors. A small time step (~$0.0002h/u_j$) is used at the beginning of simulations, and it is slowly increased. After the jet transient state, a larger time step (~$0.002h/u_j$) is used for additional 200,000 iterations, corresponding to a flow time of 400 h/u_j. Then, time-history data on points and surfaces are saved during the simulations. The total computational time for the cold jet JetTR1 is about 240,000 core hours. It should be noted that for the case with a higher temperature and jet velocity, a smaller time step is needed to maintain the CFL number. The time step can still be estimated by using the $\Delta t = 0.0002h/u_j$ but with an updated larger u_j in the hot jet cases. A small time step will lead to a longer computational time to reach the same flow time, which is important for the acoustic data analysis of hot jets.

IV. Verification and Validation

The current work is a continuation of our previous work [20], where the detailed grid convergence study, and verification and validation of numerical methods are carried out and presented. Cases tested include the acoustic pulse, shock propagation, and shock-vortex interaction. The numerical method has also been used to study the supersonic jet with relatively low temperature ratios, and results match rather well with the experiments conducted at the University of Cincinnati [10, 29]. Interested readers can refer to [20] for details.

V. Aerodynamic Results

A. Instantaneous fields

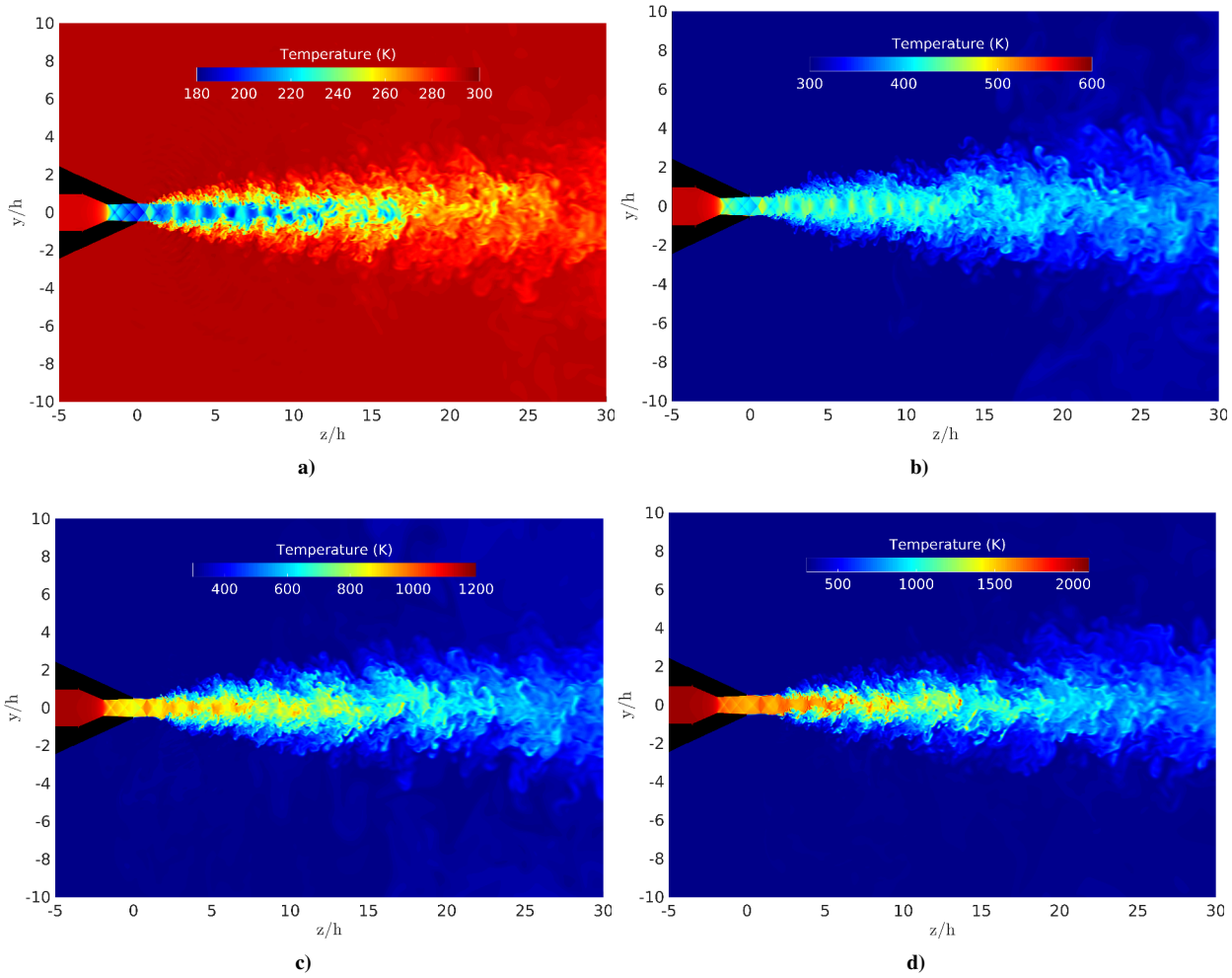

Figure 4. Instantaneous fields of static temperature for a) JetTR1, b) JetTR2, c) JetTR4, and d) JetTR7. The nozzle is in balck.

Snapshots of temperature contours for the jets with different TRs are presented in Fig. 4. Temperature drops due to the flow acceleration from subsonic to supersonic speeds can be observed clearly according to the different color bars. The nozzle exit temperature increases greatly when the jet is hot, and the mean temperatures in the first few shock cells agree well with the values calculated by one-dimensional assumption as shown in Table 1. Shock structures within the nozzle and the jet core region are also visible, especially for JetTR1. Due to the sharp edge of the nozzle throat, an oblique shock is formed when the nozzle flow passes it. It is reflected in the divergent part of the nozzle. When the over-expanded jet flows out the nozzle, another shock wave is generated at the nozzle lip due to the overexpansion. It merges with the previous internally reflected shock waves and forms the shock diamond inside the jet core. The jet shear layers provoke fast growing Kelvin-Helmholtz instabilities that promote the mixing of the jet and the ambient air. With the increase of the TR, the visible starting point of flow instabilities in the shear layer as shown in Fig. 4d, has been delayed slightly away from the nozzle exit plane, due to the fact that Re actually decreases as presented in Table

1. These unsteady structures grow spatially, evolve into chaotic motions rapidly in the downstream, and inherently decay into small-scale structures.

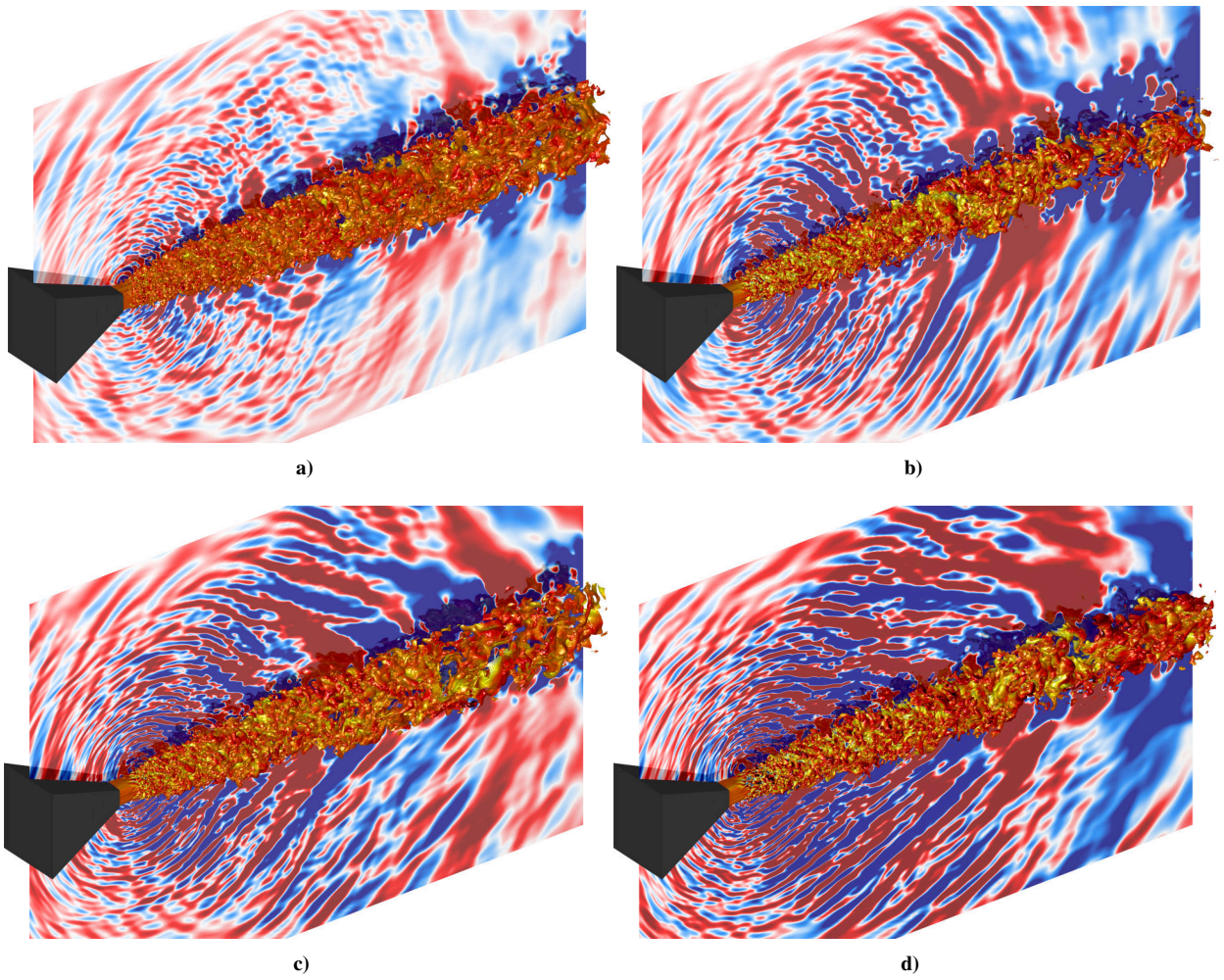

Figure 5. Instantaneous fields of acoustic pressure from $-1000Pa$ to $1000Pa$ and isosurfaces of density colored by Mach number for a) JetTR1 with $\rho = 1.0kg/m^3$, b) JetTR2 with $\rho = 0.9kg/m^3$, c) JetTR4 with $\rho = 0.8kg/m^3$, and d) JetTR7 with $\rho = 0.5kg/m^3$. The nozzle is in black.

Figs. 5 shows the three-dimensional instantaneous features of the jet shear layer and the two-dimensional near-field acoustic pressure in the minor axis plane. The jet shear layer is illustrated by isosurfaces of density. Both large and small scale turbulent structures can be observed. As for the acoustic fields for the cold jet as shown in Fig. 5a, three acoustic components of the supersonic jet in the near field can be observed. The first is the waves propagating upstream in the region close to the nozzle geometry, which is corresponding to the screech noise. The second is the circular waves radiating from certain points in the shear layers. Those waves are generated by the interactions between the shock wave and turbulent structures in the shear layers, which are also called the broadband shock associated noises. The third is the wave propagating in the downstream direction with a relatively low frequency, corresponding to the turbulent mixing noise. When TR increases as shown in Figs. 5b, 5c, and 5d, the magnitudes of the acoustic pressure fluctuations rise for all of the three acoustic components as indicated by the darkened color. Moreover, another acoustic component, Mach wave radiation, appears at about 120 - 140 degrees measured from the jet upstream direction for these hot jets. This component is generated by the wavy turbulent structures convected downstream at supersonic speeds. It can be noted that the radiation directivity also changes slightly, and this will be discussed more in the following part.

B. Mean flow fields

The properties of the jet mean flow fields are first studied. Fig. 6 shows the mean axial velocity normalized by the corresponding ideally expanded jet velocity u_j in both the minor and major axis planes. According to velocity contours and the value of u_j for each case, it can be seen that the magnitude of jet exit velocity is increased significantly for hot jets. Although the jet ideally expanded Mach number is almost the same for all the cases, the increase of axial velocity is due to the larger speed of sound caused by the elevated temperature ratios. Another feature that can be observed is that the length of the jet core region decreases when the jet becomes hot. For example, the length of the cold jet as shown in Fig. 6a is slightly larger than $z/h = 15$, whereas the length of JetTR7 is as short as $z/h = 10$ as shown in Fig. 6d. There is around 30 % reduction in the jet core region length, mainly due to the more rapid eddy decay. Moreover, evidence of axis switching in this rectangular jet can also be found from the velocity contours. For example, at the cut plane $z/h = 15$, the jet spreading rate in the minor planes is larger than or roughly the same as that in the major axis planes.

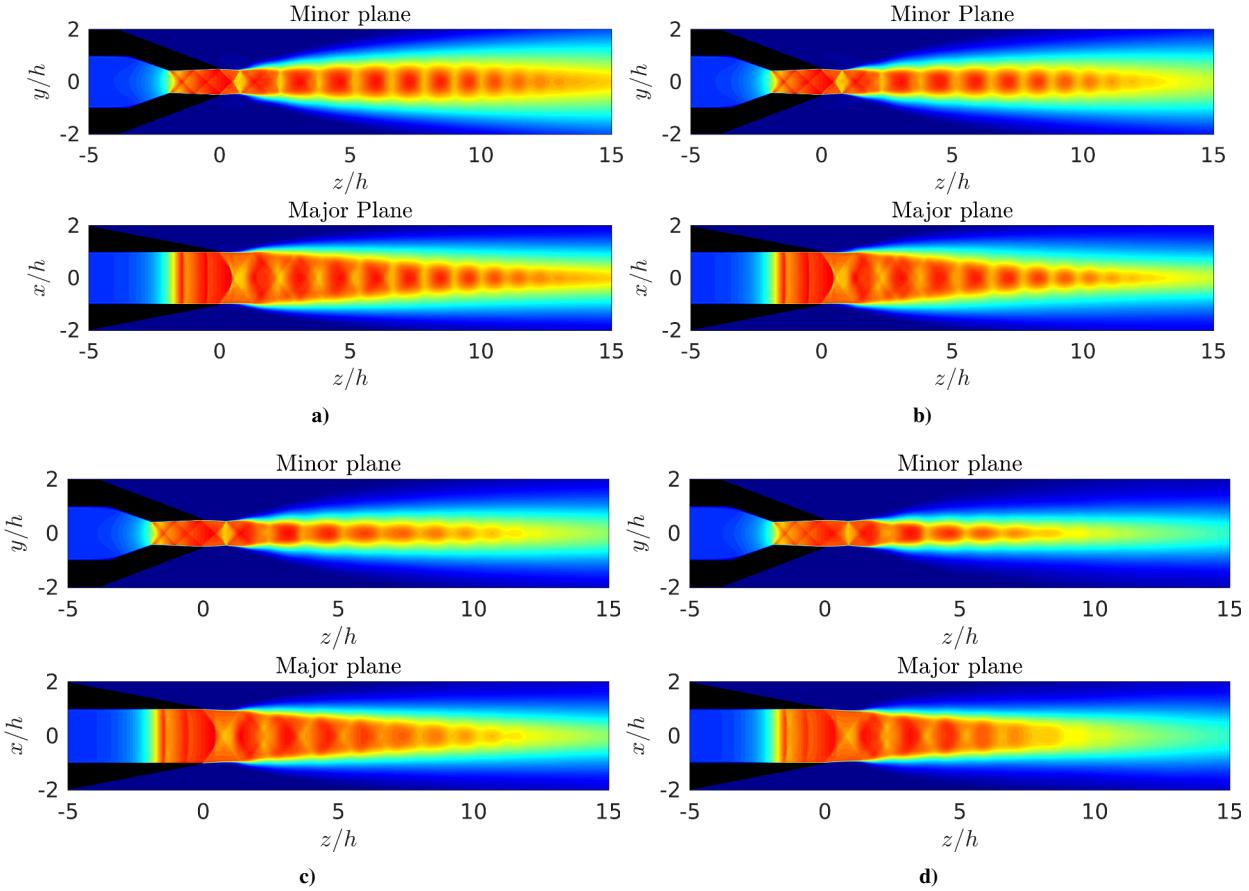

Figure 6. Mean axial veocity fields normalized by the corresponding ideally expanded jet velocity u_j for a) JetTR1, b) JetTR2, c) JetTR4, and d) JetTR7. The nozzle is in black. The color ranges from 0 (blue) to 1.3 (red) for all the cases.

An important parameter for the investigation of supersonic jet noise is the acoustic Mach number. It is defined as the ratio of the flow speed and the ambient speed of sound as Eq. 1.

$$Ma_{acoustic} = \frac{u_j}{\sqrt{\gamma R T_{ambient}}} \tag{1}$$

where u_j is the ideally expanded jet velocity, γ denotes the specific heat ratio, R is the gas constant for air, and $T_{ambient}$ is the ambient temperature. The acoustic Mach number for the different jets is computed as shown in Fig. 7. It can be found that for JetTR7 the acoustic Mach number at the nozzle exit has increased to be about 3 times of that for the cold JetTR1.

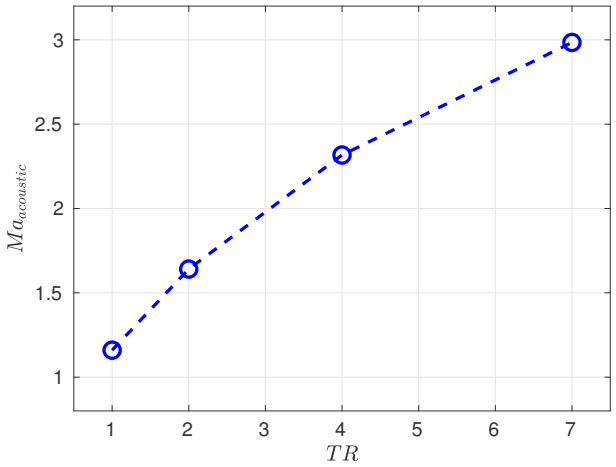

Figure 7. Acoustic Mach number for jets with different TRs.

C. Convection velocity

The convection velocity of the shear layer turbulent structures can help understand the supersonic jet sound generation mechanism, especially for the Mach wave radiation component. Based on the work of Papamoschou and Roshko [40], the convection Mach numbers in a shear layer formed by two streams are defined as :

$$Ma_{c1} = \frac{u_1 - u_c}{a_1}, Ma_{c2} = \frac{u_c - u_2}{a_2} \tag{2}$$

where Ma_c is the convection Mach number, u_c is the convection velocity, and a is the speed of sound. Subscripts 1 and 2 denote stream 1 and 2 recpectively. For flows without shock waves, the relation of the two convection velocities can be approximated as [40] :

$$Ma_{c1} = \sqrt{\frac{\gamma_2}{\gamma_1}} Ma_{c2} \tag{3}$$

where γ_1 and γ_2 are the specific heat ratios in the two streams. In the current study, the jet can be considered as stream 1 and the ambient (with subscript 0) can be put as stream 2. So we can get $u_1 = u_j$, $u_2 = u_0 = 0$, $a_1 = \sqrt{\gamma_j R T_j}$, and $a_2 = \sqrt{\gamma_0 R T_0}$. Use Eq. 2, we can rearrange Eq. 3 to get the normalized convection velocity:

$$\frac{u_c}{u_j} = \frac{1}{\sqrt{\frac{\gamma_0}{\gamma_j}\frac{a_j}{a_0}} + 1} = \frac{1}{\sqrt{TR} + 1} \tag{4}$$

Eq. 4 shows that the normalized convection velocity decreases when the jet temperature ratio increases. The estimated values of u_c/u_j are shown in Table 2. It should be noted that Eq. 4 is obtained without the consideration of shock waves in the over-expansion jet. This similar formulation has been observed to work rather well in subsonic and cold moderate compressible jets [41]. In the current over-expanded flows, neglecting the shock wave effects does not affect the trend but may affect the accuracy of the estimation.

Table 2. Nozzle operating conditions. TR is temperature ratio; u_j, T_j and a_j denote velocity, static temperature and speed of sound of the ideally expanded equivalent jet; estimated u_c/u_j is the estimated normalized convection velocity using Eq. 4; LES $\overline{u_c/u_j}$ and LES $\overline{M_c}$ are the normalized average convection velocity and acoustic convection Mach number computed from the simulation data in the minor axis plane up to $z = 5h$.

Case	TR	$u_j(m \cdot s^{-1})$	$T_j(K)$	$a_j(m \cdot s^{-1})$	estimated u_c/u_j	LES $\overline{u_c/u_j}$	LES $\overline{M_c}$
JetTR1	1.0	399	214	293	0.50	0.81	0.95
JetTR2	2.0	564	430	415	0.41	0.75	1.24
JetTR4	4.0	801	888	586	0.33	0.68	1.60
JetTR7	7.0	1070	1607	774	0.27	0.62	1.88

With the saved simulation data, the local convection velocity along the shear layers in both the minor and major planes can be computed using cross-correlations of axial velocity fluctuations. The computed results are plotted in

Fig. 8. Figs. 8a and 8c show the normalized convection velocity, u_c/u_j, of the turbulent structures in the shear layers in the minor and major axis planes, whereas Figs. 8b and 8d show their acoustic convection Mach numbers, $M_c = u_c/c_0$, of the shear layers in the minor and major axis planes. Due to the interaction between the shock waves and shear layers, the convection velocity varies along the axial direction. It can be found that the magnitude of the normalized convection velocity decreases when the jet temperature increases, which is consistent with the previous trend prediction by Eq. 4. However, there are discrepancies between the prediction by the simplified formula and the computed values from the simulation data as shown in Table 2. As expected previously, this is mainly due to the shock wave effect is neglected in Eq. 4. Regarding the acoustic convection Mach number, $\overline{Mc}$, as listed in Table 2, it compares the convection velocity of the turbulent structure in the shear layer with the ambient speed sound, which is a useful parameter that can be used to estimate the directivity of Mach wave radiations. Apart from JetTR1 with a subsonic acoustic convection Mach number 0.94, all the other three cases have a supersonic acoustic convection Mach number and it increases with the jet temperature. Furthermore, it can also be seen that the convection velocities in the major axis plane are smaller than those in the minor plane, which indicates a different Mach wave radiation angle in the major plane.

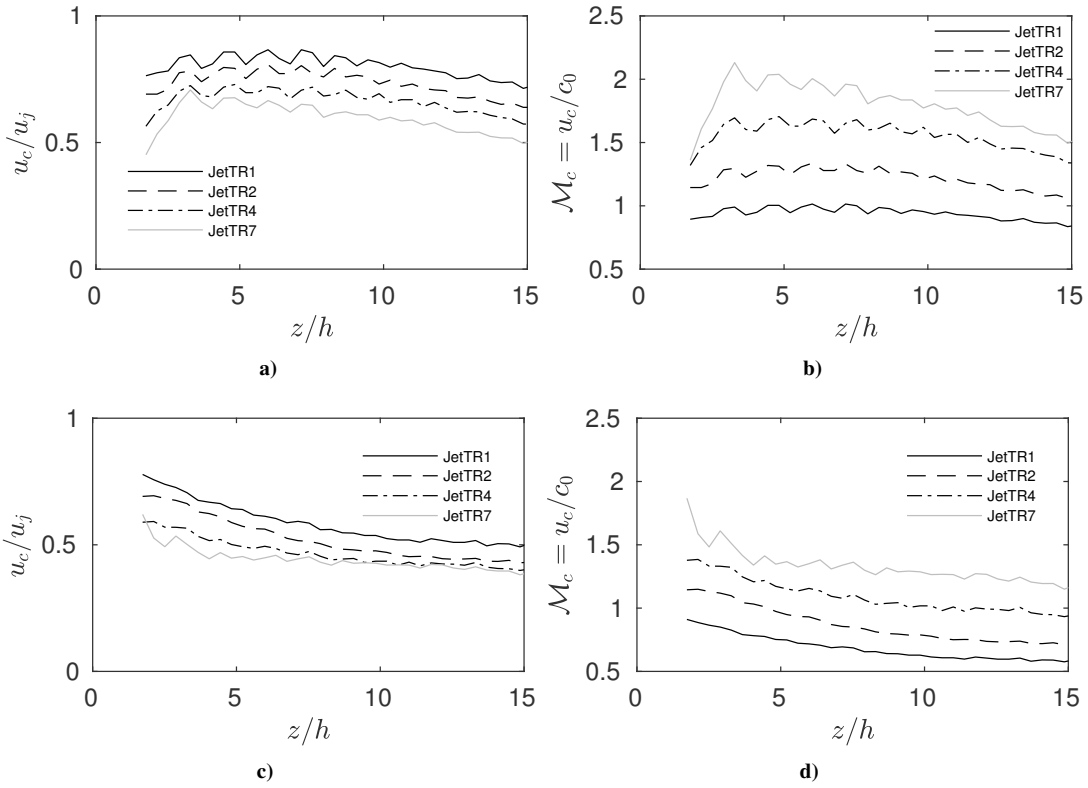

Figure 8. Normalized convection velocity a,c) and acoustic convection Mach number b,d) of the turbulent structure along the jet shear layer in the minor axis plane a,b) and in the major axis plane c,d).

VI. Acoustic Results

A. Near-field acoustic

The OASPL obtained at both the minor and major axis planes near the jet are shown in Fig. 9. It can be seen from the contours that the OASPL has been increased in all directions when the jet temperature is high. The maximum OASPL for each jet is around 200 dB, 210 dB, 220 dB and 230 dB respectively. Another significant feature is that the Mach wave radiation component (at about 120 degrees measured from the jet upstream direction) becomes much stronger when the jet temperature is increased.

The pressure spectra obtained in the vicinity of the nozzle at (x, y, z)=(0, $2h$, $-2h$) are shown in Fig. 10 as functions of the Strouhal number $St = fD_{eq}/u_j$. It can be observed that there is a dominant frequency for these jets at Strouhal number ranging from 0.25 to 0.38, as shown in Table 3. These dominant frequencies are the screech components propagating in the upstream direction. Except for JetTR2, no visible harmonic frequencies of the screech

tone can be found. When the jet temperature increases, the amplitude of this screech component first increases from 150 dB/St for JetTR1 to 160 dB/St for JetTR2, then it slightly decreases and maintains at around 159 dB/St for both JetTR4 and JetTR7. In the work of Mora et al. [10], they found an overall decrease of the amplitude of the screech component when the jet temperature is high. Our previous numerical work presented in [20] found a contradictory trend where the amplitude of the screech component increased with the jet temperature. In that work, constant gas properties, c_p and γ, were used for all the jets, where different shear layer structures and turbulent quantities were provided. This seems to be the reason for the contradictory trend. However, more work is needed to clarify it.

Tam [42] proposed a model to predict the screech frequency for rectangular and non-axisymmetric jets. For the current rectangular nozzle, this model can be expressed as :

$$St_{Tam} = \frac{\frac{D_{eq}u_c/u_j}{2h(1+u_c/a_0)(M_j^2-1)^{1/2}}[(h_j/b_j)^2+1]^{1/2}}{\left\{\left[\frac{1+\frac{\gamma-1}{2}M_j^2}{1+\frac{\gamma-1}{2}M_d^2}\right]^{(\gamma+1)/(2(\gamma-1))}\frac{M_d}{M_j}-1\right\}\frac{b}{b+h}+1} \tag{5}$$

where h and b are the height and width of the rectangular jet at the exit plane, h_j and b_j are the height and width of the ideally expanded jet whose formulas can be found in [42], $M_d = 1.5$ stands for the nozzle design Mach number, M_j is the ideally expanded jet Mach number. The computed values using Eq. 5 are listed in Table 3. For comparison, the experimental results of the screech tones for JetTR1 and JetTR2 are also included. It can be seen that the simulation results agree pretty well with the experimental data, and Tam's formula also provides a good estimation in general.

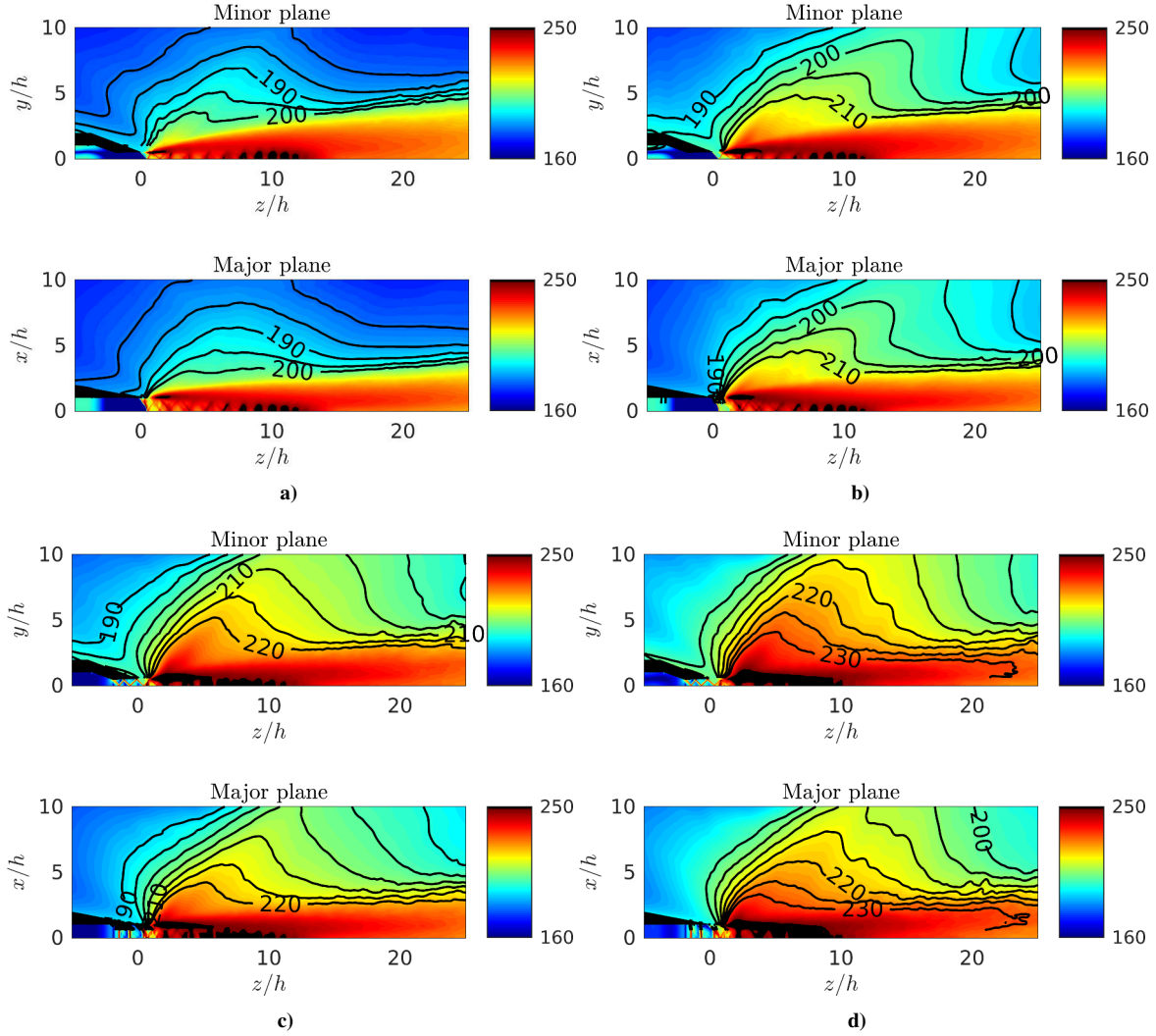

Figure 9. Near field overall sound pressure level (OASPL) for a) JetTR1, b) JetTR2, c) JetTR4, and d)JetTR7.

Table 3. Peak values for the pressure spectra at (x, y, z)=(0, $2h$, $-2h$). TR is temperature ratio; $St_{screech}$ and $dB_{screech}$ are the Strouhal number and the sound pressure level at the peak.

Case	TR	$St_{screech}$	$dB_{screech}$	$St_{screech}$ exp.	St_{Tam}
JetTR1	1.0	0.37	150	0.37	0.41
JetTR2	2.0	0.31	160	0.31	0.33
JetTR4	4.0	0.26	159	–	0.26
JetTR7	7.0	0.25	159	–	0.20

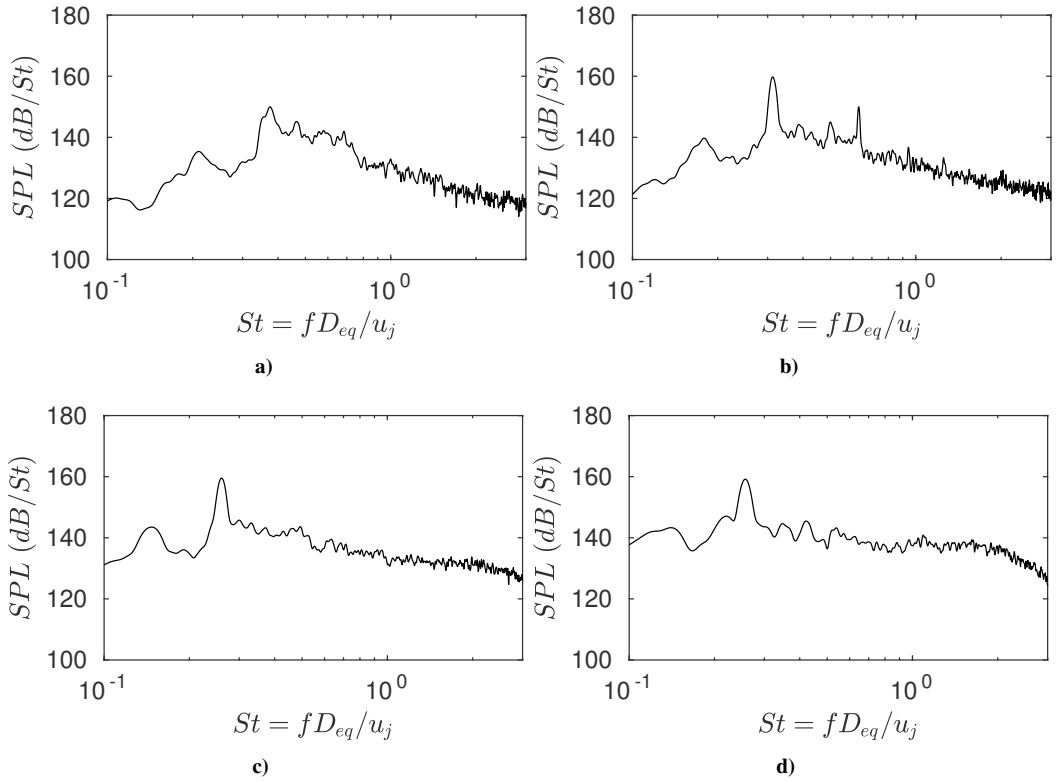

Figure 10. Pressure spectra at (x, y, z)=(0, $2h$, $-2h$) for a) JetTR1, b) JetTR2, c) JetTR4, and d)JetTR7.

B. Mach wave radiation

Mach wave radiation is a unique noise component of supersonic jets, which is generated by the large-scale turbulent structures in the jet shear layer convected downstream at supersonic speeds. It has a directivity that is closely related to the acoustic convection Mach number of turbulent structures. The pressure fluctuation contours as shown in Fig. 11 illustrate the Mach wave radiation in both the minor and major planes. For the cold jet in Figs. 11a and 11b, the Mach wave radiation cannot be observed, which is consistent with the subsonic acoustic convection Mach number 0.95 as shown in Table 2. When the jet temperature ratio increases to 2.0 and 4.0, this noise component starts to show by strong pressure fluctuations with a cone shape in both the minor and major axis planes. When the jet temperature increases to 7.0 as shown in Figs. 11g and 11h, the Mach waves becomes quite apparent. It can also be found that the minor axis plane has a stronger Mach wave radiation than the major axis plane.

Another feature of the Mach wave radiation under the effect of jet temperature comes from the propagation direction. With the increase of the jet temperature from TR = 2 to TR = 7, it can be seen in Fig. 11 that the propagation direction slightly inclines more close to the side direction. This slight difference can be observed by looking at the area with $z/h = 5 - 10$ and $y/h = 8 - 10$ for example. Stronger pressure fluctuations can be seen in this area. The propagation angle measured from the jet upstream direction can be estimated by using the acoustic convection Mach number, M_c.

$$\theta = 180 - arccos(\frac{1}{M_c}) \tag{6}$$

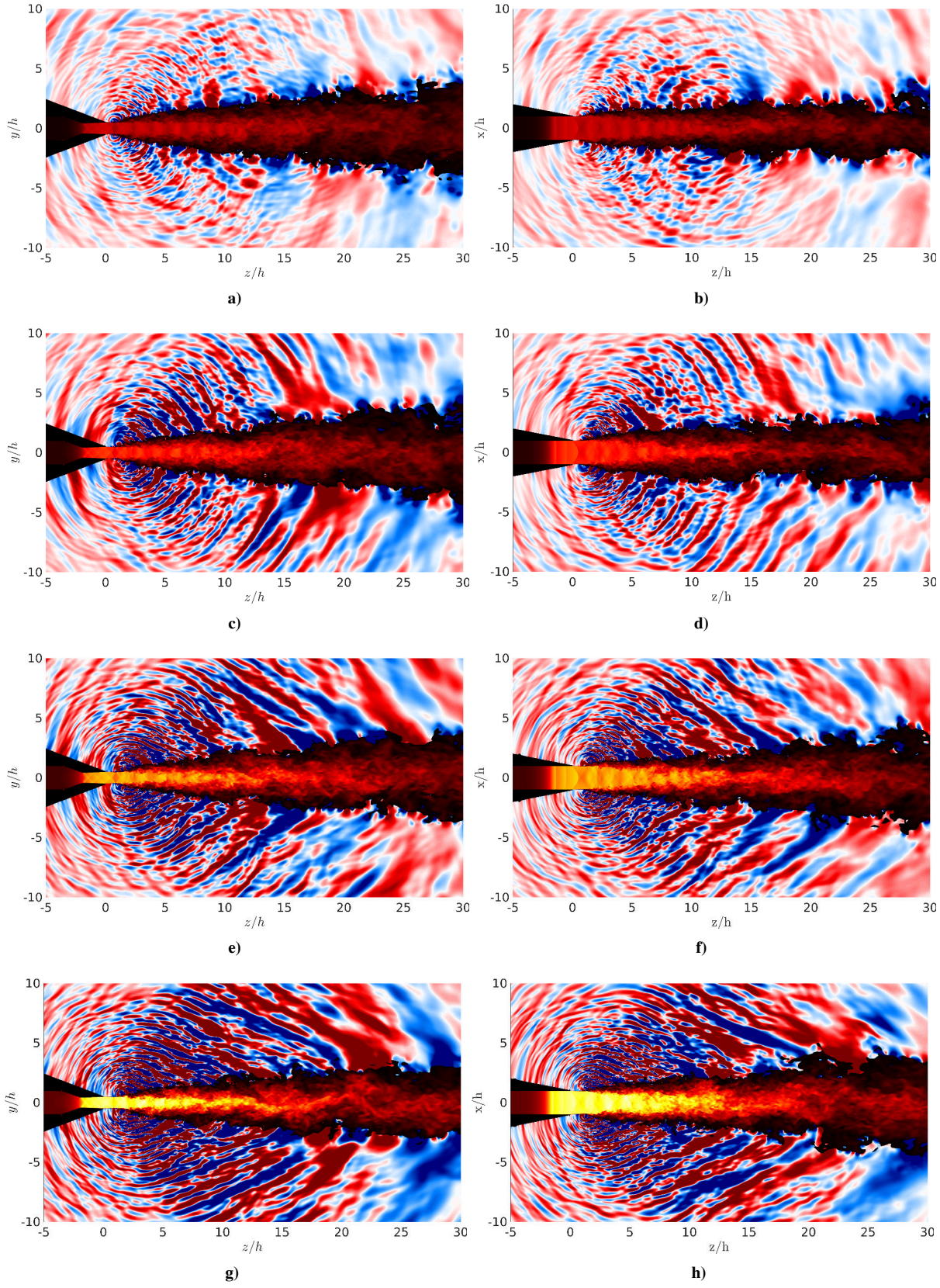

Figure 11. Near field fluctuating pressure and jet acoustic convection Mach number contours for a,b) JetTR1, c,d) JetTR2, e,f) JetTR4, and g,h)JetTR7. The left column is in the minor axis plane and the right column is in the major axis plane.

Using the simulation averaged acoustic convection Mach number $\overline{M}_c$ from Table 2, the propagation direction angle can be estimated by Eq. 6. It should be noted that $\overline{M}_c$ for JetTR1 is subsonic, 0.95, which explains why there is no Mach wave radiation observed in Figs. 11a and 11b. For the other three cases, the Mach wave radiation angle can be estimated to be 144, 129, and 122 degrees respectively. The relative smaller propagation angle, e.g. 124 degrees for JetTR7, indicates a Mach wave radiation inclining more close to the side direction, which is consistent with the results shown in the contours.

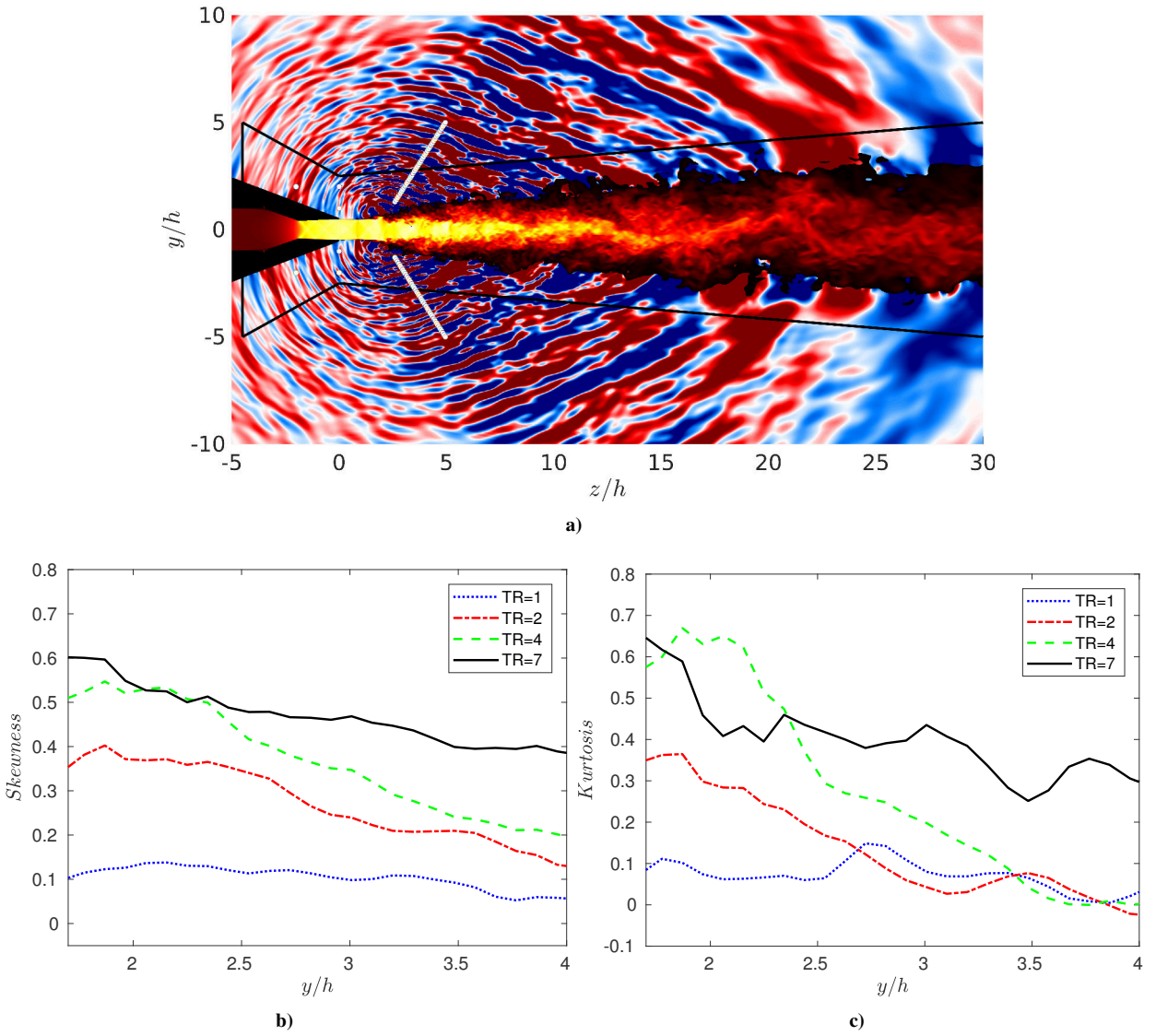

Figure 12. a) Point probes location in white dots, b) skewness, and c)kurtosis.

For heated supersonic jets, crackle noise first investigated by Ffowcs Williams et al. [43] may occur. This noise component is very annoying for observers [46]. It is characterized by intermittent positive pressure spikes, which consists of a strong compression followed by a relaxation. Crackle noise propagates downstream along the Mach wave radiation direction and accounts for about 30% of the overall sound pressure level in this direction [44, 45]. There are two parameters commonly used to identify the crackle noise. The first one is skewness of pressure signals [46]. It is defined as:

$$S = \frac{E[(p(t) - \overline{p}(t))^3]}{\sigma^3} \tag{7}$$

where E stands for the expected value, $p(t)$ and $\overline{p}(t)$ are pressure signal and its mean value, σ denotes the standard deviation of the pressure signal. If the skewness exceeds 0.4, it indicates that the crackle noise component exists,

while there is no crackle noise if the skewness is smaller than 0.3 [46]. Another statistic parameter is Kurtosis, which is useful for evaluating the crackle or the nonlinear effect. The Kurtosis is defined as:

$$S = \frac{E[(p(t) - \overline{p}(t))^4]}{\sigma^4} - 3 \tag{8}$$

Kurtosis quantifies the distribution of a signal relative to a Gaussian distribution. Kurtosis with a value of zero means the shape of the signal is the same as the Gaussian distribution. A positive kurtosis indicates a steep waveform while a negative kurtosis indicates a flat waveform compared with the Gaussian distribution.

Point probes are placed along the Mach wave direction, as shown in Fig. 12a, to save the time history data during the simulations. The skewness and kurtosis factors of these points are calculated and plotted in Figs. 12b and 12c. It can be seen that the skewness of the cold jet JetTR1 is very low with a value of around 0.1. When the jet temperature increases, the skewness is increased as well. For JetTR2, the skewness value within the monitored range is smaller than 0.4. For JetTR4, the points in the region close to the jet core with $y/h < 2.7$ have a skewness value larger than 0.4, which indicates the presence of the crackle noise. However, it then decays to smaller values when the Mach wave further propagates. For JetTR7, skewness maintains a value larger than 0.4 in the whole monitored range. In general, when the point probe location is away from the jet region, there is a trend that the skewness decreases for the hot jets. Moreover, according to the threshold value of 0.4 to identify the crackle noise component as mentioned previously, both JetTR4 and JetTR7 have the crackle noise. A similar trend can be found in the profiles of the kurtosis factor. JetTR1 has the minimum kurtosis among the cases presented. It has a value of around zero, which indicates its probability density function is close to the Gaussian distribution. When the jet temperature increases, large positive kurtosis factors are observed forJetTR2, JetTR4 and JetTR7, especially in the region close to the jet core. These large values indicate that they have very steep pressure waveforms.

C. Far-field acoustic

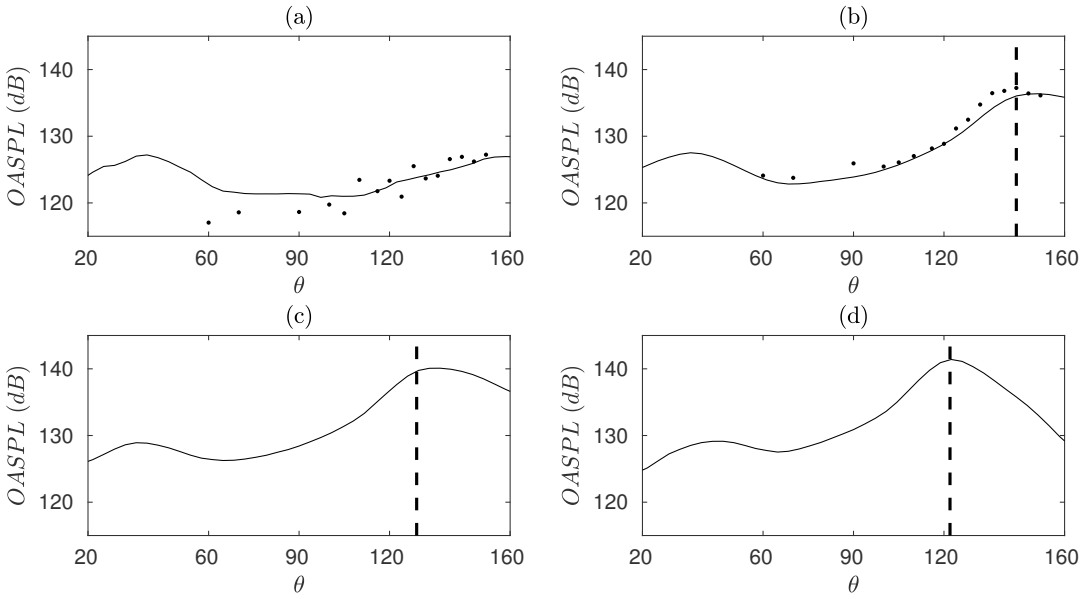

Figure 13. OASPL obtained on the circle of radius $40D_{eq}$ as function of the angle θ with respect to the upstrea direction for (a)JetTR1, (b)JetTR2, (c)JetTR4, and (d)JetTR7; • experimental results and ___ LES results. The vertical dash lines show the Mach wave radiation angles of 144, 129, and 122 degrees estimated previously.

Far-field acoustic characteristics of the jets are computed by using Ffowcs Williams-Hawkings (FW-H) acoustic analogy. The axisymmetric FW-H surface is shown in Fig. 12a by the solid black lines. The OASPL at a distance of $40D_{eq}$ (the circle center is at the nozzle exit center) in the far-field is plotted along different angles θ as shown in Fig. 13. For the JetTR1 and JetTR2, overall good agreements between the experimental data and simulation results have been achieved. When the temperature is increased, the OASPL in the far-field does not change much in the upstream direction at the angle ranging from 20 to 50 degrees. In the side direction around 90 degrees, an increase of the OASPL can be observed for the high-temperature jets. In the downstream direction where θ is around 130 degrees, a significant increase of OASPL is found for JetTR2, JetTR4, and JetTR7. Those correspond to the Mach wave radiations. For this

peak, there is a slight shift of the peak angle to the upstream direction for hot jets. These peak angles also match rather well with the previously estimated angles with Eq. 6: 144, 129, and 122 degrees for JetTR2, JetTR4, and JetTR7, as plotted by vertical dash lines in Fig. 13.

VII. Conclusion

A rectangular supersonic nozzle with a temperature ratio of up to 7.0 has been numerically studied using large eddy simulations in the current work. To account for the gas properties in the high-temperature regime, a pre-calculated table for temperature-dependent specific heat ratio and specific heat at constant pressure has been implanted into the flow solver with the consideration of the chemical equilibrium assumption. When the jet temperature is increased, the jet exit velocity is drastically elevated, although the ideally expanded jet Mach number is still the same. The jet core region is found to be shortened, while the jet convection velocity in the shear layer is greatly increased. The near-field acoustic results show that the overall sound pressure level for the hot jet is increased in all the directions (i.e. the upstream, side direction, and downstream). A very strong Mach wave radiation has been observed in the hot jet. The analysis of pressure skewness and kurtosis factors show that the crackle noise component exists for JetTR4 and JetTR7. The acoustic convection Mach number turns out to be a good parameter to estimate the directivity of Mach wave radiation, and the predicted values agree very well with both the near-field and far-field acoustic results.

Acknowledgements

The computations were performed on resources provided by the Swedish National Infrastructure for Computing (SNIC) at PDC Centre for High Performance Computing (PDC-HPC). The first author also would like to thank Dr. Stefan Wallin for the assistance of the code modification and implementations.

References

[1] Hiley, P., Wallacet, H., and Booz, D., "Nonaxisymmetric Nozzles Installed in Advanced Fighter Aircraft," *Journal of Aircraft*, Vol. 13, No. 12, 1976, pp. 1000–1006.

[2] Viswanath, K., Johnson, R., Corrigan, A., Kailasanath, K., Mora, P., Baier, F., and Gutmark, E., "Flow Statistics and Noise of Ideally Expanded Supersonic Rectangular and Circular Jets," *AIAA Journal*, 2017, pp. 1–15.

[3] Gutmark, E. and Grinstein, F., "Flow Control with Noncircular Jets," *Annual Review of Fluid Mechanics*, Vol. 31, No. 1, 1999, pp. 239–272.

[4] Tam, C. K., "Supersonic Jet Noise," *Annual Review of Fluid Mechanics*, Vol. 27, No. 1, 1995, pp. 17–43.

[5] Bailly, C. and Fujii, K., "High-Speed Jet Noise," *Mechanical Engineering Reviews*, Vol. 3, No. 1, 2016, pp. 15–00496.

[6] Gojon, R. and Bogey, C., "Numerical Study of the Flow and the Near Acoustic Fields of an Underexpanded Round Free Jet Generating Two Screech Tones," *International Journal of Aeroacoustics*, Vol. 16, No. 7-8, 2017, pp. 603–625.

[7] Harper-Bourne, M. and Fisher, M. J., "The Noise from Shock Waves in Supersonic Jets," AGARD-CP-131, 1973.

[8] Powell, A., "On the Mechanism of Choked Jet Noise," *Proceedings of the Physical Society. Section B*, Vol. 66, No. 12, 1953, pp. 1039.

[9] Powell, A., "The Noise of Choked Jets," *The Journal of the Acoustical Society of America*, Vol. 25, No. 3, 1953, pp. 385–389.

[10] Mora, P., Baier, F., Kailasanath, K., and Gutmark, E. J., "Acoustics from a Rectangular Supersonic Nozzle Exhausting over a Flat Surface," *The Journal of the Acoustical Society of America*, Vol. 140, No. 6, 2016, pp. 4130–4141.

[11] Wall, A. T., Gee, K. L., James, M. M., Bradley, K. A., McInerny, S. A., and Neilsen, T. B., "Near-Field Noise Measurements of a High-Performance Military Jet Aircraft," *Noise Control Engineering Journal*, Vol. 60, No. 4, 2012, pp. 421–434.

[12] Tam, C. K. and Ganesan, A., "Modified $k - \varepsilon$ Turbulence Model for Calculating Hot Jet Mean Flows and Noise," *AIAA Journal*, Vol. 42, No. 1, 2004, pp. 26–34.

[13] Tam, C. K., Pastouchenko, N. N., and Viswanathan, K., "Fine-Scale Turbulence Noise from Hot Jets," *AIAA Journal*, Vol. 43, No. 8, 2005, pp. 1675.

[14] Davey, R. F. and Roshko, A., "The Effect of a Density Difference on Shear-Layer Instability," *Journal of Fluid Mechanics*, Vol. 53, No. 3, 1972, pp. 523–543.

[15] Gutmark, E., Schadow, K., and Wilson, K., "Effect of Convective Mach Number on Mixing of Coaxial Circular and Rectangular Jets," *Physics of Fluids A: Fluid Dynamics*, Vol. 3, No. 1, 1991, pp. 29–36.

[16] Doty, M. and McLaughlin, D. K., "Two-Point Correlations of Density Gradient Fluctuations in High Speed Jets Using Optical Deflectometry," AIAA Paper, 2002-0367, 2002.

[17] Viswanathan, K., "Aeroacoustics of Hot Jets," *Journal of Fluid Mechanics*, Vol. 516, 2004, pp. 39–82.

[18] De Cacqueray, N. and Bogey, C., "Noise of an Overexpanded Mach 3.3 Jet: Non-Linear Propagation Effects and Correlations with Flow," *International Journal of Aeroacoustics*, Vol. 13, No. 7-8, 2014, pp. 607–632.

[19] Langenais, A., Vuillot, F., Troyes, J., and Bailly, C., "Numerical Investigation of the Noise Generated by a Rocket Engine at Lift-Off Conditions Using a Two-Way Coupled CFD-CAA Method." AIAA Paper, 2017-3212, 2017.

[20] Gojon, R., Baier, F., Gutmark, E., and Mihaescu, M., "Temperature Effects on the Aerodynamic and Acoustic Fields of a Rectangular Supersonic Jet," AIAA Paper, 2017-0002, 2017.

[21] Liu, J., Corrigan, A., Kailasanath, K., and Taylor, B., "Impact of the Specific Heat Ratio on Noise Generation in a High-Temperature Supersonic Jet," AIAA Paper, 2016-2125, 2016.

[22] Liu, J., Corrigan, A. T., Kailasanath, K., and Gutmark, E. J., "Effects of Temperature on Noise Generation in Supersonic Jets," AIAA Paper, 2016-2937, 2016.

[23] Liu, J., Kailasanath, K., and Gutmark, E. J., "Similarity Spectra Analysis in Highly Heated Supersonic Jets Using Large-Eddy Simulations," AIAA Paper, 2017-0926, 2017.

[24] Neilsen, T. B., Gee, K. L., Wall, A. T., and James, M. M., "Similarity Spectra Analysis of High-Performance Jet Aircraft Noise," *The Journal of the Acoustical Society of America*, Vol. 133, No. 4, 2013, pp. 2116–2125.

[25] Tam, C. K. and Parrish, S. A., "Noise of High-Performance Aircraft at Afterburner," *Journal of Sound and Vibration*, Vol. 352, 2015, pp. 103–128.

[26] Chu, B.-T. and Kovásznay, L. S., "Non-Linear Interactions in a Viscous Heat-Conducting Compressible Gas," *Journal of Fluid Mechanics*, Vol. 3, No. 5, 1958, pp. 494–514.

[27] Gojon, R., Gutmark, E., and Mihaescu, M., "On the Response of a Rectangular Supersonic Jet to a Near-Field Located Parallel Flat Plate," AIAA Paper, 2017-3018, 2017.

[28] Heeb, N., Mora, P., Gutmark, E., and Kailasanath, K., "Investigation of the Noise from a Rectangular Supersonic Jet," AIAA Paper, 2013-2239, 2013.

[29] Mora, P., Baier, F., Gutmark, E. J., and Kailasanath, K., "Acoustics from a Rectangular C-D Nozzle Exhausting over a Flat Surface," AIAA Paper, 2016-1884, 2016.

[30] Baier, F., Mora, P., Gutmark, E. J., and Kailasanath, K., "Flow Measurements from a Supersonic Rectangular Nozzle Exhausting Over a Flat Surface," AIAA Paper, 2017-0932, 2017.

[31] https://www.grc.nasa.gov/www/CEAWeb.

[32] Eliasson, P., "EDGE: A Navier-Stokes Solver for Unstructured Grids," 2001.

[33] Semlitsch, B., Mihaescu, M., Fuchs, L., and Gutmark, E. J., "Large Eddy Simulations of Microjets Impact on Supersonic Jet Exiting a CD Conical Nozzle," AIAA Paper, 2013-2039, 2013.

[34] Semlitsch, B., Mihaescu, M., Fuchs, L., and Gutmark, E., "Analyzing the Impact of the Inlet Temperature on the Acoustic Noise Production form a Supersonic Jet Using Large Eddy Simulations," *Proceedings of Meetings on Acoustics ICA2013*, Vol. 19, ASA, 2013, p. 030011.

[35] Margolin, L. G. and Rider, W. J., "A Rationale for Implicit Turbulence Modelling," *International Journal for Numerical Methods in Fluids*, Vol. 39, No. 9, 2002, pp. 821–841.

[36] Margolin, L., Rider, W., and Grinstein, F., "Modeling Turbulent Flow with Implicit LES," *Journal of Turbulence*, Vol. 7, No. N15, 2006.

[37] Fureby, C. and Grinstein, F., "Monotonically Integrated Large Eddy Simulation of Free Shear Flows," *AIAA Journal*, Vol. 37, No. 5, 1999, pp. 544–556.

[38] Jameson, A., Schmidt, W., and Turkel, E., "Numerical Solution of the Euler Equations by Finite Volume Methods Using Runge-Kutta Time-Stepping Schemes," AIAA Paper, 1981-1259, 1981.

[39] Ducros, F., Ferrand, V., Nicoud, F., Weber, C., Darracq, D., Gacherieu, C., and Poinsot, T., "Large-Eddy Simulation of the Shock/Turbulence Interaction," *Journal of Computational Physics*, Vol. 152, No. 2, 1999, pp. 517–549.

[40] Papamoschou, D. and Roshko, A., "The Compressible Turbulent Shear Layer: An Experimental Study," *Journal of Fluid Mechanics*, Vol. 197, 1988, pp. 453–477.

[41] Gojon, R., Bogey, C., and Marsden, O., "Investigation of Tone Generation in Ideally Expanded Supersonic Planar Impinging Jets Using Large-Eddy Simulation," *Journal of Fluid Mechanics*, Vol. 808, 2016, pp. 90–115.

[42] Tam, C., "The Shock-Cell Structures and Screech Tone Frequencies of Rectangular and Non-Axisymmetric Supersonic Jets," *Journal of Sound and Vibration*, Vol. 121, No. 1, 1988, pp. 135–147.

[43] Williams, J. F., Simson, J., and Virchis, V., "Crackle: An Annoying Component of Jet Noise," *Journal of Fluid Mechanics*, Vol. 71, No. 2, 1975, pp. 251–271.

[44] Krothapalli, A., Venkatakrishnan, L., and Lourenco, L., "Crackle: A Dominant Component of Supersonic Jet Mixing Noise," AIAA Paper, 2000-2024, 2000.

[45] Krothapalli, A., Arakeri, V., and Greska, B., "Mach Wave Radiation: A Review and an Extension," AIAA Paper, 2003-1200, 2003.

[46] Nichols, J. W., Lele, S. K., Ham, F. E., Martens, S., and Spyropoulos, J. T., "Crackle Noise in Heated Supersonic Jets," *Journal of Engineering for Gas Turbines and Power*, Vol. 135, No. 5, 2013, pp. 051202.